Available online at www.sciencedirect.com
ScienceDirect
Journal of Power Sources 161 (2006) 949–956
JOURNAL OF POWER SOURCES
www.elsevier.com/locate/jpowsour

Effects of cathode humidification on the gas–liquid interface location in a PEM fuel cell

Chun-I Lee [1], Hsin-Sen Chu *

Department of Mechanical Engineering, National Chiao Tung University, Hsinchu 300, Taiwan, ROC

Received 25 March 2006; received in revised form 5 May 2006; accepted 8 May 2006
Available online 11 July 2006

Abstract

This study investigates the location of the gas–liquid interface under various humidity conditions in the cathode gas diffusion layer and the conventional flow field of a polymer electrolyte membrane fuel cell (PEMFC), using commercial computational fluid dynamics (CFDRC) analysis, based on a three-dimensional steady state isothermal model. The effects of the formation of liquid water on the transport of reactant gas are considered in the model. The simulation results indicate that the gas–liquid interface approaches the gas flow channel inlet and the cell performance declines gradually as liquid water obstructs the pores in the porous media as the relative humidity of the cathode is increased. Additionally, the oxygen fraction, the water fraction and the liquid water saturation field along the flow channel are presented.

Keywords: PEM fuel cell; Conventional flow channel; Performance; Humidity; CFDRC

1. Introduction

Proton exchange membrane fuel cells (PEMFCs) are promising new energy conversion devices because of their high efficiency, simplicity of design and operation and environmental friendliness. However, the performance and efficiency of this PEM fuel cell must be improved further to make it cost-effective for use in these applications [1–3]. Accordingly, water management is critical to the proper operation of PEM fuel cells. However, over the past decade, effective water management has remained elusive. During operation, formed liquid water is transported within the membrane–electrode assembly, and controlling its motion is extremely difficult. When the rate of generation of water at the cathode by electro-osmotic drag and the oxygen reduction reaction exceeds the water removal rate from the cathode by back-diffusion to the anode, evaporation, and capillary transport of liquid water through the cathode diffusion layer and catalyst layer, the cathode becomes flooded. Additionally, excess accumulated liquid water blocks the gas pores in the diffusion layer and the catalyst layer, which are needed for the transport of oxygen gas, and form a barrier over the catalyst active surface in the catalyst layer, worsening the performance.

Springer et al. [4,5] developed a 1D isothermal model to predict the net water per proton flux ratio across the membrane in PEMFCs. However, this model cannot evaluate the decrease in reactants and the accumulation of products in the flow direction. Fuller et al. [6] and Nguyen et al. [7] proposed a 2D heat transport and water transport model to account for the distribution of water and the net water flux within the membrane, at various operating temperatures and membrane hydration along the flow channels. Yi et al. [8] modified Nguyen's model to describe both liquid and gas phase distributions along the flow paths on the anode-side and the cathode-side in a PEMFC. The results indicated that anode humidification improved the conductivity of the membrane, and that the cell performance was enhanced by the injection of liquid water and the increase in humidification temperature.

In Refs. [9,10], Mazumder et al. developed a 3D model to predict the effect of the formation of liquid water on the performance of the PEMFC. In Ref. [9], the polarization behavior was overestimated, based on the assumption that no liquid water was formed. In contrast, when liquid water was present, the condensation and/or evaporation of water via equilibrium phase transformation proceeded as described in Ref. [10]. Since water

* Corresponding author. Tel.: +886 3 5712121x55141; fax: +886 3 5727930.
E-mail address: hschu@cc.nctu.edu.tw (H.-S. Chu).
[1] Graduate student.

0378-7753/$ – see front matter © 2006 Elsevier B.V. All rights reserved.
doi:10.1016/j.jpowsour.2006.05.012

Nomenclature

C	mass fraction
C_F	quadratic drag factor
D	mass diffusivity ($m^2\ s^{-1}$)
F	Faraday constant ($C\ mol^{-1}$)
I	current density ($A\ m^{-2}$)
k_c	condensation rate constant (s^{-1})
k_e	evaporation rate constant ($atm^{-1}\ s^{-1}$)
k_p	permeability (m^2)
M	molecular weight ($kg\ mol^{-1}$)
P	pressure (atm)
R	universal gas constant ($J\ mol^{-1}\ K^{-1}$)
S	source term
T	temperature (K)
u	velocity in the x-direction ($m\ s^{-1}$)
v	velocity in the y-direction ($m\ s^{-1}$)
V	operating voltage (V)
w	velocity in the z-direction ($m\ s^{-1}$)
x_w	molar fraction of water
Z_f	spices valence

Greek letters

α	transfer coefficient for the reaction
ε	porosity
λ	water content of membrane
ρ	density ($kg\ cm^{-3}$)
σ	ionic conductivity of the ionomer ($\Omega^{-1}\ m^{-1}$)
τ	tortuosity of diffusion layer
υ	viscosity of flow ($kg\ m^{-1}\ s^{-1}$)
Φ	phase potential (V)

Subscripts

a	anode
c	cathode
channel	flow channel
CL	catalyst layer
eff	effective
GDL	gas diffusion layer
in	inlet
k	kth component of fuel reactant
Mem; m	membrane
sat	saturated
x	X-direction
y	Y-direction
z	Z-direction

Superscripts

a	anode
c	cathode
ref	reference

condensation can obstruct pores and reduce cell performance, the polarization behavior of PEMFC must be accurately predicted to prevent such a situation. Restated, the consideration of liquid water transport substantially enhances the ability to predict cell performance, and improves the consistency between the experimental data and simulation results, especially at high current densities.

Wang et al. [11] proposed a multiphase mixing model to study two-phase water transport in the cathode. Their results revealed that the formation of liquid water influences the performance of the cell. Nevertheless, the overall PEMFC simulations could not be understood further because they considered only the cathode-side. You et al. [12] presented a 2D two-phase flow mixture model to analyze the flow and transport in the cathode of the PEMFC, and to predict the phase change and the water/oxygen distribution in both the flow channels and the porous diffusion layer. Also, such a two-phase model provides actual characteristics of the flow and the transport of reaction gas for thermal/water management.

More recently, computational fluid dynamics (CFD) have utilized water-transport models to better predict cell performance at high loads. Yan et al. [13,14] presented a 2D numerical model for the reactant gas transport phenomena and cell performance with baffle effects in the flow channel of the bipolar plate. The effects of the baffle width are explored. Additionally, the effects of liquid water formation on the reactant gas transport are taken into account in the modeling and examined in the analysis.

Recently, most of the research on the humidification conditions has focused on cell performance [8,15,16]. Studies in this area reveal that the relative humidity critically affects cell performance. As pointed out by Natarajan et al. [16], the performance of the cell increases as the relative humidity of the cathode decreases.

This study investigates the location of the interface when the liquid water began to condense along the flow channel of PEMFCs; its contribution to the cell performance is also discussed. Additionally, the resulting oxygen and water fraction distributions and liquid water saturation fields at fixed cathode humidity were obtained to validate the simulation results. All equations were solved using the commercial computational fluid dynamics (CFDRC) software to simulate this system.

2. 3D mathematical model of PEMFC

Fig. 1 schematically depicts the 3D PEMFC system employed in this study. It consists of the anode flow channel, the anode diffusion layer, the anode catalyst layer, the proton exchange membrane, the cathode catalyst layer, the cathode diffusion layer and the cathode flow channel. Table 1 presents the geometrical and physical parameters adopted in the present simulation; some minor parameters are omitted and can be found elsewhere [10,18,19]. In this study, the inlet fuel, hydrogen, is assumed to be fully humidified on the anode-side; the operating pressure is 1 atm and the operating temperature is 343 K. The objective is to investigate the location of the interface when the liquid water begins to condense along the flow channel of PEMFCs. The following simplifying assumptions are made: (1) the gaseous phase of the working fluid behaves as an ideal gas and the liquid water is incompressible; (2) the Reynolds number of the fluid is below 100 because the velocity of the mixture is low, and the flow is considered to be laminar; (3) the diffusion layer, the catalyst

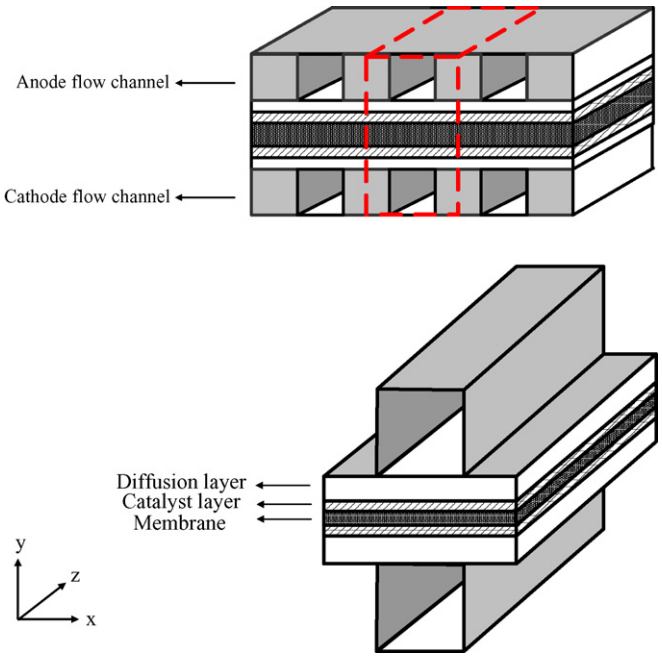

Fig. 1. Schematic diagram of 3D PEMFC.

Table 1
Geometric and physical parameters in the simulation

Channel length (m)	0.07112
Channel height (m)	7.62×10^{-4}
Channel width (m)	7.62×10^{-4}
Diffuser layer thickness (m)	3×10^{-4}
Catalyst layer thickness (m)	1×10^{-5}
Membrane thickness (m)	3×10^{-5}
Porosity of diffuser layer	0.4
Permeability of diffuser layer (m^2)	1.76×10^{-11}
Porosity of catalyst layer	0.4
Permeability of catalyst layer (m^2)	1.76×10^{-11}
Porosity of membrane	0.28
Permeability of membrane (m^2)	1.18×10^{-18}
Operation temperature (K)	343
Operation pressure (atm)	1
Anode fuel	Hydrogen
Cathode fuel	Air
Hydrogen stoichiometric flow rate	1.5
Air stoichiometric flow rate	3
Relative humidity of the anode (%)	100

layer and the membrane are isotropic and homogeneous, and characterized by an effective permeability and uniform porosity; (4) the system operates in a steady and isothermal state; (5) negligible heat is generated.

Based on these assumptions, the basic gas transport equations for a general 3D PEMFC are as follows:

- Continuity equation:

$$\frac{\partial u}{\partial x} + \frac{\partial v}{\partial y} + \frac{\partial w}{\partial z} = 0 \tag{1}$$

- Momentum equations:

$$\varepsilon_{\text{eff}} \left(u\frac{\partial u}{\partial x} + v\frac{\partial u}{\partial y} + w\frac{\partial u}{\partial z} \right) = -\frac{\varepsilon_{\text{eff}}}{\rho}\frac{\partial P}{\partial x} + \upsilon\varepsilon_{\text{eff}} \left(\frac{\partial^2 u}{\partial x^2} + \frac{\partial^2 u}{\partial y^2} + \frac{\partial^2 u}{\partial z^2} \right) + S_u \tag{2}$$

$$\varepsilon_{\text{eff}} \left(u\frac{\partial v}{\partial x} + v\frac{\partial v}{\partial y} + w\frac{\partial v}{\partial z} \right) = -\frac{\varepsilon_{\text{eff}}}{\rho}\frac{\partial P}{\partial y} + \upsilon\varepsilon_{\text{eff}} \left(\frac{\partial^2 v}{\partial x^2} + \frac{\partial^2 v}{\partial y^2} + \frac{\partial^2 v}{\partial z^2} \right) + S_v \tag{3}$$

$$\varepsilon_{\text{eff}} \left(u\frac{\partial w}{\partial x} + v\frac{\partial w}{\partial y} + w\frac{\partial w}{\partial z} \right) = -\frac{\varepsilon_{\text{eff}}}{\rho}\frac{\partial P}{\partial z} + \upsilon\varepsilon_{\text{eff}} \left(\frac{\partial^2 w}{\partial x^2} + \frac{\partial^2 w}{\partial y^2} + \frac{\partial^2 w}{\partial z^2} \right) + S_w \tag{4}$$

- Species concentration equation:

$$\varepsilon_{\text{eff}} \left(u\frac{\partial C_k}{\partial x} + v\frac{\partial C_k}{\partial y} + w\frac{\partial C_k}{\partial z} \right) = D_{k,\text{eff}} \left(\frac{\partial^2 C_k}{\partial x^2} + \frac{\partial^2 C_k}{\partial y^2} + \frac{\partial^2 C_k}{\partial z^2} \right) + S_c + S_{\text{L}} \tag{5}$$

Table 2 presents expressions for the source terms S_u, S_v, S_w and S_c in the above equations. Within the table, the parameters ε_{eff}, C_{F}, k_{p} and Z_{f} are the effective porosity, the quadratic drag factor, the permeability and the valence of the species, respectively;

Table 2
Expressions for the source terms in the governing equations

	S_u	S_v	S_w	S_c
Flow channel	0	0	0	-
Diffuser layer	$-\frac{\upsilon\varepsilon^2}{k_{\text{p}}}u - \frac{\varepsilon^3 C_{\text{F}}\rho u}{\sqrt{k_{\text{p}}}}\sqrt{u^2+v^2+w^2}$	$-\frac{\upsilon\varepsilon^2}{k_{\text{p}}}v - \frac{\varepsilon^3 C_{\text{F}}\rho v}{\sqrt{k_{\text{p}}}}\sqrt{u^2+v^2+w^2}$	$-\frac{\upsilon\varepsilon^2}{k_{\text{p}}}w - \frac{\varepsilon^3 C_{\text{F}}\rho w}{\sqrt{k_{\text{p}}}}\sqrt{u^2+v^2+w^2}$	0
Catalyst layer	$-\frac{\upsilon\varepsilon^2}{k_{\text{p}}}u - \frac{\varepsilon_{\text{eff}}^3 C_{\text{F}}\rho u}{\sqrt{k_{\text{p}}}}\sqrt{u^2+v^2+w^2}$	$-\frac{\upsilon\varepsilon^2}{k_{\text{p}}}v - \frac{\varepsilon_{\text{eff}}^3 C_{\text{F}}\rho v}{\sqrt{k_{\text{p}}}}\sqrt{u^2+v^2+w^2}$	$-\frac{\upsilon\varepsilon^2}{k_{\text{p}}}w - \frac{\varepsilon_{\text{eff}}^3 C_{\text{F}}\rho w}{\sqrt{k_{\text{p}}}}\sqrt{u^2+v^2+w^2}$	$\text{H}_2: -\frac{1}{2FC_{\text{a}}}j_{\text{a}}$, $\text{O}_2: -\frac{1}{4FC_{\text{c}}}j_{\text{c}}$, $\text{H}_2\text{O}: \frac{1}{2FC_{\text{c}}}j_{\text{c}}$
Membrane	$-\frac{\upsilon\varepsilon^2}{k_{\text{p}}}u - \frac{\varepsilon_{\text{eff}}^3 C_{\text{F}}\rho u}{\sqrt{k_{\text{p}}}}\sqrt{u^2+v^2+w^2} + \frac{k_{\text{p}}}{\upsilon}Z_{\text{f}}C_{\text{H}^+}F\cdot\nabla\Phi\frac{\partial u}{\partial x}$	$-\frac{\upsilon\varepsilon^2}{k_{\text{p}}}v - \frac{\varepsilon_{\text{eff}}^3 C_{\text{F}}\rho v}{\sqrt{k_{\text{p}}}}\sqrt{u^2+v^2+w^2} + \frac{k_{\text{p}}}{\upsilon}Z_{\text{f}}C_{\text{H}^+}F\cdot\nabla\Phi\frac{\partial v}{\partial y}$	$-\frac{\upsilon\varepsilon^2}{k_{\text{p}}}w - \frac{\varepsilon_{\text{eff}}^3 C_{\text{F}}\rho w}{\sqrt{k_{\text{p}}}}\sqrt{u^2+v^2+w^2} + \frac{k_{\text{p}}}{\upsilon}Z_{\text{f}}C_{\text{H}^+}F\cdot\nabla\Phi\cdot\frac{\partial w}{\partial z}$	$\frac{ZF}{RT}D_{k,\text{eff},\text{H}^+}\cdot C_{\text{H}^+}\left(\frac{\partial^2\Phi}{\partial x^2}+\frac{\partial^2\Phi}{\partial y^2}+\frac{\partial^2\Phi}{\partial z^2}\right)$

$D_{k,\mathrm{eff}} = D_k \varepsilon^{\tau_i}$ represents the effective diffusion coefficient of the kth component of fuel reactant [17]; j_a and j_c are defined as:

$$j_\mathrm{a} = A j_0^{\mathrm{ref}} \left(\frac{C_{\mathrm{H_2}}}{C_{\mathrm{H_2}}^{\mathrm{ref}}}\right) \left[\mathrm{e}^{(\alpha_\mathrm{a} F/RT)\eta} - \frac{1}{\mathrm{e}^{(\alpha_\mathrm{c} F/RT)\eta}}\right] \tag{6}$$

$$j_\mathrm{c} = A j_0^{\mathrm{ref}} \left(\frac{C_{\mathrm{O_2}}}{C_{\mathrm{O_2}}^{\mathrm{ref}}}\right) \left[\mathrm{e}^{(\alpha_\mathrm{a} F/RT)\eta} - \frac{1}{\mathrm{e}^{(\alpha_\mathrm{c} F/RT)\eta}}\right] \tag{7}$$

The phase potential equation yields the local current density distributions:

$$\frac{\partial}{\partial x}\left(\sigma_\mathrm{m}\frac{\partial \Phi}{\partial x}\right) + \frac{\partial}{\partial y}\left(\sigma_\mathrm{m}\frac{\partial \Phi}{\partial y}\right) + \frac{\partial}{\partial z}\left(\sigma_\mathrm{m}\frac{\partial \Phi}{\partial z}\right) = S_j \tag{8}$$

where Φ and σ_m represent the phase potential and the ionic conductivity of the membrane.

The relationships between the phase potential Φ and the current density i can be expressed as,

$$i_x = -\sigma_\mathrm{m}\frac{\partial \Phi}{\partial x}; \qquad i_y = -\sigma_\mathrm{m}\frac{\partial \Phi}{\partial y}; \qquad i_z = -\sigma_\mathrm{m}\frac{\partial \Phi}{\partial z} \tag{9}$$

Then, Eq. (8) can be rewritten as

$$\frac{\partial i_x}{\partial x} + \frac{\partial i_y}{\partial y} + \frac{\partial i_z}{\partial z} = S_j \tag{10}$$

In the membrane, the ionic conductivity σ_m is strongly related to the water content λ. It is defined as the ratio of the number of water molecules to the number of charge sites [4]:

$$\sigma_\mathrm{m}(T) = \sigma_\mathrm{m}^{\mathrm{ref}} \exp\left[1268\left(\frac{1}{303} - \frac{1}{T}\right)\right] \tag{11}$$

$$\sigma_\mathrm{m}^{\mathrm{ref}} = 0.005139\lambda - 0.00326 \tag{12}$$

The empirical relationship between the water content in the membrane and the partial pressure of the water is,

$$\lambda = \begin{cases} 0.043 + 17.81a - 39.85a^2 + 36.0a^3 & 0 \le a \le 1 \\ 14 + 1.4(a-1) & 1 < a \le 3 \end{cases} \tag{13}$$

where a is the water activity and is given by,

$$a = \frac{x_\mathrm{w} P}{P_\mathrm{sat}} \tag{14}$$

In the above equation, the saturation pressure varies with the temperature and can be determined from the thermodynamic table or using the following empirical expression:

$$P_\mathrm{sat} = 10^{-2.1794 + 0.02953T - 9.1837\times10^{-5}T^2 + 1.4454\times10^{-7}T^3} \tag{15}$$

During the operation of the fuel cell, the partial pressure of the water in the electrode may exceed its saturation pressure if the local concentration of water is high. Accordingly, liquid water may form and occupy the pores in the porous media. Operating the cell at a high reaction rate may cause severe mass transport overpotential because the diffusing species are blocked. Furthermore, extremely small pores in the porous media cause capillary forces to dominate the transport of liquid water. However, the actual expression of this force cannot be formulated. Eq. (16) models the equilibrium phase change. This approach has also been adopted by Nguyen et al. [17], and is the same approach being used in current study, because it allows natural extension to the finite-rate phase change.

The determination of liquid water condensation or evaporation capacity can be denoted as S_L [10]:

$$S_\mathrm{L} = \begin{cases} Mk_\mathrm{c}\dfrac{\varepsilon_\mathrm{eff} x_\mathrm{w}}{RT}(x_\mathrm{w}P - P_\mathrm{sat}), & \text{if } x_\mathrm{w}P > P_\mathrm{sat} \\ k_\mathrm{e}\varepsilon_\mathrm{eff} s\rho(x_\mathrm{w}P - P_\mathrm{sat}), & \text{if } x_\mathrm{w}P < P_\mathrm{sat} \end{cases} \tag{16}$$

where k_c and k_e are the condensation and evaporation rate constants, respectively. s is the saturation of liquid water, and is defined as the ratio of liquid volume to the volume of the pores. $x_\mathrm{w}P$ is the partial pressure of water vapor, and x_w is the molar fraction of water vapor. The saturation pressure of water is P_sat, and can be computed using the curve-fitted expressions provided by Springer et al. [4].

2.1. Boundary conditions

Wang et al. [11] indicated that although the gas in the GDL is transported by diffusion, some convection with a very low velocity also occurs. Therefore, the boundary conditions in this work are expressed as general expressions. In this work, the operating temperature and pressure are set to 343 K and 1 atm, respectively. A constant flow configuration was used with gas fluxes of 1.5 and 3 times the stoichiometric value at 1 A cm^{-2} for H_2 and air, respectively.

At the gas channel inlet,

$$\text{anode}: \quad u = 0,\ v = 0,\ w = w_\mathrm{in}^\mathrm{a},\ C_{\mathrm{H_2}} = C_{\mathrm{H_2,in}}^\mathrm{a},$$
$$C_{\mathrm{H_2O}} = C_{\mathrm{H_2O,in}}^\mathrm{a} \tag{17}$$

$$\text{cathode}: \quad u = 0,\ v = 0,\ w = w_\mathrm{in}^\mathrm{c},\ C_{\mathrm{O_2}} = C_{\mathrm{O_2,in}}^\mathrm{c},$$
$$C_{\mathrm{H_2O}} = C_{\mathrm{H_2O,in}}^\mathrm{c},\ C_{\mathrm{N_2}} = C_{\mathrm{N_2,in}}^\mathrm{c} \tag{18}$$

At the interfaces between the channel walls and plate collectors,

$$u = v = w = \frac{\partial C_k}{\partial x} = 0 \tag{19}$$

At the interfaces between the gas channels and the gas diffuser layer,

$$\varepsilon_{\mathrm{eff,GDL}}\left.\frac{\partial u}{\partial y}\right|_{y=Y_\mathrm{GDL}} = \left.\frac{\partial u}{\partial y}\right|_{y=Y_\mathrm{channel}},$$
$$\varepsilon_{\mathrm{eff,GDL}}\left.\frac{\partial v}{\partial y}\right|_{y=Y_\mathrm{GDL}} = \left.\frac{\partial v}{\partial y}\right|_{y=Y_\mathrm{channel}},$$
$$\varepsilon_{\mathrm{eff,GDL}}\left.\frac{\partial w}{\partial y}\right|_{y=Y_\mathrm{GDL}} = \left.\frac{\partial w}{\partial y}\right|_{y=Y_\mathrm{channel}}, \quad u_{y=Y_\mathrm{GDL}} = u_{y=Y_\mathrm{channel}},$$
$$v_{y=Y_\mathrm{GDL}} = v_{y=Y_\mathrm{channel}}, \quad w_{y=Y_\mathrm{GDL}} = w_{y=Y_\mathrm{channel}},$$
$$\varepsilon_{\mathrm{eff,GDL}}\left.\frac{\partial C_k}{\partial y}\right|_{y=Y_\mathrm{GDL}} = \left.\frac{\partial C_k}{\partial y}\right|_{y=Y_\mathrm{channel}},$$
$$C_{k,y=Y_\mathrm{GDL}} = C_{k,y=Y_\mathrm{channel}} \tag{20}$$

At the interfaces between the gas diffuser layer and the catalyst layer,

$$\varepsilon_{\text{eff,GDL}} \left.\frac{\partial u}{\partial y}\right|_{y=Y_{\text{GDL}}} = \varepsilon_{\text{eff,CL}} \left.\frac{\partial u}{\partial y}\right|_{y=Y_{\text{CL}}},$$

$$\varepsilon_{\text{eff,GDL}} \left.\frac{\partial v}{\partial y}\right|_{y=Y_{\text{GDL}}} = \varepsilon_{\text{eff,CL}} \left.\frac{\partial v}{\partial y}\right|_{y=Y_{\text{CL}}},$$

$$\varepsilon_{\text{eff,GDL}} \left.\frac{\partial w}{\partial y}\right|_{y=Y_{\text{GDL}}} = \varepsilon_{\text{eff,CL}} \left.\frac{\partial w}{\partial y}\right|_{y=Y_{\text{CL}}}, \quad u_{y=Y_{\text{GDL}}} = u_{y=Y_{\text{CL}}},$$

$$v_{y=Y_{\text{GDL}}} = v_{y=Y_{\text{CL}}}, \quad w_{y=Y_{\text{GDL}}} = w_{y=Y_{\text{CL}}},$$

$$\varepsilon_{\text{eff,GDL}} \left.\frac{\partial C_k}{\partial y}\right|_{y=Y_{\text{GDL}}} = \varepsilon_{\text{eff,CL}} \left.\frac{\partial C_k}{\partial y}\right|_{y=Y_{\text{CL}}},$$

$$C_{k,y=Y_{\text{GDL}}} = C_{k,y=Y_{\text{CL}}} \tag{21}$$

At the interfaces between the catalyst layer and the membrane,

$$\varepsilon_{\text{eff,CL}} \left.\frac{\partial u}{\partial y}\right|_{y=Y_{\text{CL}}} = 0, \quad \varepsilon_{\text{eff,CL}} \left.\frac{\partial v}{\partial y}\right|_{y=Y_{\text{CL}}} = 0,$$

$$\varepsilon_{\text{eff,CL}} \left.\frac{\partial w}{\partial y}\right|_{y=Y_{\text{CL}}} = 0, \quad u_{y=Y_{\text{CL}}} = 0,$$

$$v_{y=Y_{\text{CL}}} = 0, \quad w_{y=Y_{\text{CL}}} = 0, \quad \varepsilon_{\text{eff,CL}} \left.\frac{\partial C_k}{\partial y}\right|_{y=Y_{\text{CL}}} = 0 \tag{22}$$

The effect of liquid water upon cell performance is investigated. Proton transport and the electro-osmotic phenomenon cause liquid water to be transported in the proton exchange membrane. Therefore, in elucidating the transport of liquid water, the velocity, the flux and the shear stress at the catalyst layer and the membrane interface must be considered to be continuously distributed. Additionally, the saturation concentration of liquid water, C_{S}, and the concentration flux must be continuous. Therefore, the following boundary conditions were applied.

$$\varepsilon_{\text{eff,MEM}} \left.\frac{\partial u}{\partial y}\right|_{y=Y_{\text{MEM}}} = \varepsilon_{\text{eff,CL}} \left.\frac{\partial u}{\partial y}\right|_{y=Y_{\text{CL}}},$$

$$\varepsilon_{\text{eff,MEM}} \left.\frac{\partial v}{\partial y}\right|_{y=Y_{\text{MEM}}} = \varepsilon_{\text{eff,CL}} \left.\frac{\partial v}{\partial y}\right|_{y=Y_{\text{CL}}},$$

$$\varepsilon_{\text{eff,MEM}} \left.\frac{\partial w}{\partial y}\right|_{y=Y_{\text{MEM}}} = \varepsilon_{\text{eff,CL}} \left.\frac{\partial w}{\partial y}\right|_{y=Y_{\text{CL}}}, \quad u_{y=Y_{\text{MEM}}} = u_{y=Y_{\text{CL}}},$$

$$v_{y=Y_{\text{MEM}}} = v_{y=Y_{\text{CL}}}, \quad w_{y=Y_{\text{MEM}}} = w_{y=Y_{\text{CL}}},$$

$$\varepsilon_{\text{eff,MEM}} \left.\frac{\partial C_{\text{S}}}{\partial y}\right|_{y=Y_{\text{MEM}}} = \varepsilon_{\text{eff,CL}} \left.\frac{\partial C_{\text{S}}}{\partial y}\right|_{y=Y_{\text{CL}}},$$

$$C_{\text{S},y=Y_{\text{MEM}}} = C_{\text{S},y=Y_{\text{CL}}} \tag{23}$$

At the gas channel outlet, the fully developed flow conditions are assumed to be

$$u = \frac{\partial w}{\partial z} = v = \frac{\partial C_k}{\partial z} = 0 \tag{24}$$

The boundary conditions of phase potential at the interface between the catalyst layer and the membrane is,

$$\Phi_{\text{CL}} = \Phi_{\text{MEM}}, \qquad \varepsilon_{\text{eff, CL}} \frac{\partial \Phi_{\text{CL}}}{\partial y} = \frac{\partial \Phi_{\text{MEM}}}{\partial y} \tag{25}$$

3. Results and discussion

In this study, the location of the gas–liquid interface along the flow channel direction at various cathode humidity conditions and its effect on cell performance were elucidated by modeling a 3D PEMFC system using CFDRC. Fig. 2 shows the effect of the relative humidity of the cathode on the location of the interface where the liquid water begins to condense along the flow channel at a cell operating voltage of 0.7 V. The interface is defined as the location where liquid water begins to condense. The horizontal dotted line indicates the interface between the flow channel and the gas diffusion layer. A higher cathode relative humidity corresponds to a smaller distance between the gas–liquid interface and the gas inlet, as clearly displayed in Fig. 2(a). Furthermore, the gas–liquid interface moves to the flow channel inlet as the relative humidity of the cathode increases. This phenomenon is caused by: (i) the decrease in the amount of evaporated water through the flowing gas stream; (ii) the increase in the partial pressure of water and the ability to reach the saturation pressure of the vapor water relatively quickly to form liquid water earlier as the relative humidity of the cathode increases. On the contrary, the gas–liquid interface moves closer to the catalyst layer when the relative humidity of the cathode is less than 60%, as shown in Fig. 2(b). In conclusion, increasing the relative humidity of the cathode can reposition the gas–liquid interface and cause liquid water to appear, affecting the performance of the cell, because

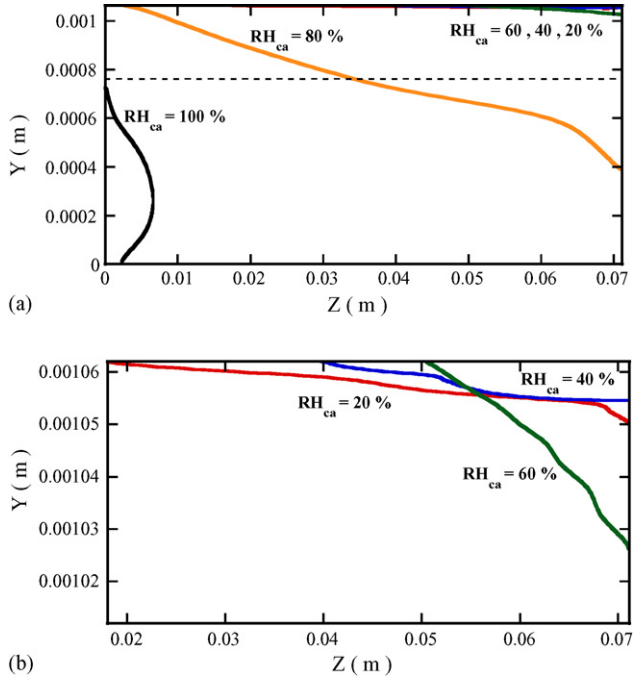

Fig. 2. Effects of relative humidity of cathode on the location of the interface where liquid water begins to condense along the flow channel at a cell operating voltage of 0.7 V. (a) RH_{ca} = 20–100% and (b) RH_{ca} = 20–60%.

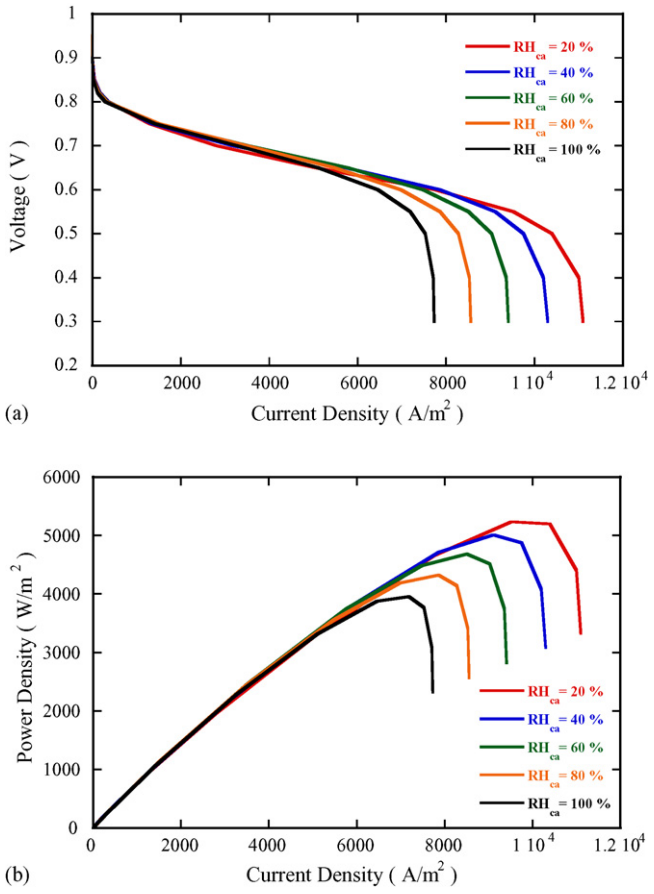

Fig. 3. Effect of relative humidity of the cathode on cell performance at cell operating voltage of 0.7 V. (a) *I–V* curves and (b) *I–P* curves.

liquid water may occupy the pores in the porous media, reducing the amount of fuel gas that can reach the catalyst layer.

Fig. 3(a) and (b) plot *I–V* and *I–P* curves at various relative humidities of the cathode at an operating voltage of 0.7 V. The results in Fig. 3(a) reveal that the cell performance decreases as the relative humidity of the cathode increases, because the amount of liquid water increases with the relative humidity. Accordingly, the pores in the porous media were obstructed by liquid water at the cathode-side, reducing the amount of reaction gas to the catalyst layer. Therefore, the performance of the cell gradually decreases. Also, the polarization curves do not seem to vary as the relative humidity of the cathode increases, at an operating voltage that exceeds ~0.65 V. A large voltage results in a small current density, and therefore, a relatively small electrochemical reaction rate. However, the performance of the cell decreases significantly as the operating voltage declines below the ~0.65 V operating voltage, since a large current density accelerates the rate of the electrochemical reaction. In particular, in Fig. 3(a), the higher cathode relative humidity (100%) offers a better cell performance than the lower one (20%) at an operating voltage of over ~0.65 V, because the rate of the electrochemical reaction decreases as the operating voltage increases. Therefore, the water content of the membrane in the initial stage increases with the relative humidity. Thus, the cell performance is improved as the relative humidity of the cathode increases.

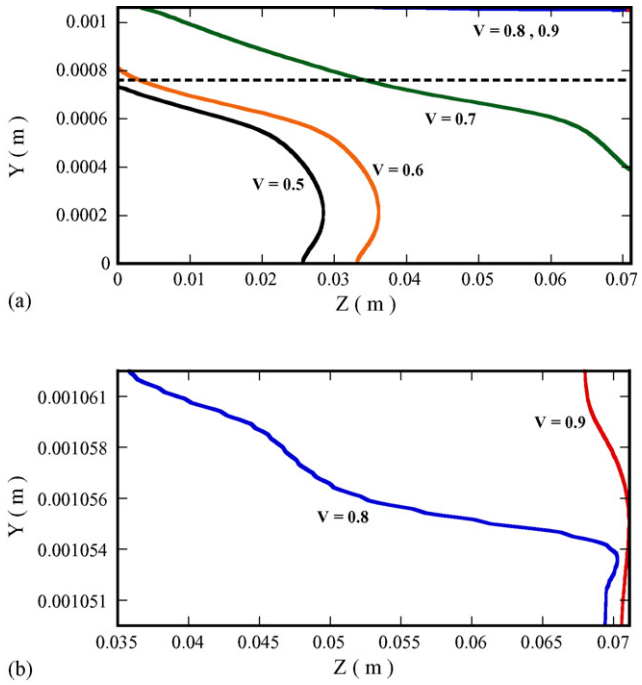

Fig. 4. Effect of cell operating voltage on the location of the interface where liquid water begins to condense along the flow channel at a relative humidity of the cathode of 80%. (a) $V = 0.5$–0.9; (b) $V = 0.8$–0.9.

By contrast, at operating voltages of below ~0.65 V, the cell performance improves as the relative humidity of the cathode decreases, because accelerating the electrochemical reaction produces more water, increasing the water content in the membrane at a low cathode relative humidity, such as 20%. However, at a high relative humidity, flooding may occur on the cathode-side. Additionally, the power density increases as the relative humidity of the cathode decreases, as shown in Fig. 3(b).

Fig. 4 shows the effects of various operating voltages on the location of the gas–liquid interface along the flow channel at a relative humidity of the cathode of 80%. Fig. 4 reveals that the gas–liquid interface is close to the catalyst layer at a high operating voltage, indicating that less water is generated at a lower electrochemical reaction rate. However, since more water is generated at a high electrochemical reaction rate, the gas–liquid interface is close to the gas diffusion layer and the flow channel at a low operating voltage. In closing, the gas–liquid interface gradually moves to the gas inlet as the operating voltage decreases, because reducing the operating voltage increases the current density. Therefore, the electrochemical reaction rate increases.

Figs. 5 and 6 plot the oxygen and water fractions in the gas flow channel and the gas diffusion layer, respectively, of the cathode-side in the direction of the flow channel at an operating voltage of 0.7 V and relative humidity of the cathode at 80%. Larger oxygen fraction appears in the gas inlet, and then gradually decreases in the flow direction, as shown in Fig. 5. The results reveal that the decrease in the oxygen fraction is caused by the catalyst layer consuming more oxygen on the cathode-side. Hence, the oxygen fraction is lowest near the catalyst layer. By contrast, Fig. 6 reveals that the water fraction gradually increases along the flow direction, because of the production of water in the

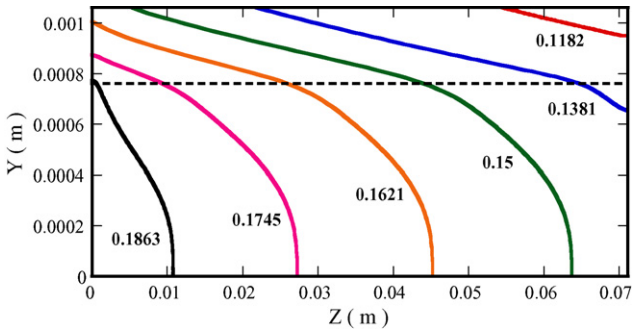

Fig. 5. Oxygen fraction in the cathode gas channel and gas diffusion layer along the flow channel at a cell voltage of 0.7 V and a relative humidity of the cathode of 80%.

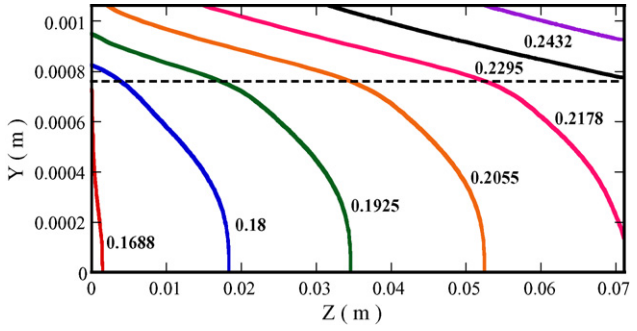

Fig. 6. Water fraction in the cathode gas channel and the gas diffusion layer along the flow channel at a cell voltage of 0.7 V and a relative humidity of the cathode of 80%.

catalyst layer of the cathode by the electrochemical reaction, as well as the transport of water from the anode-side to the cathode-side by electro-osmotic drag. Accordingly, the water fraction is the highest near the catalyst layer. Since the water mass fraction is higher near the catalyst layer, where the corresponding water partial pressure exceeds the saturated vapor pressure, causing the formation of liquid water. Therefore, Fig. 7 shows the liquid water saturation field in the gas channel and the gas diffusion layer of the cathode-side at an operating voltage of 0.7 V and a relative humidity of the cathode of 80%. The figure shows that saturation of the liquid water increases along the flow channel, because the electrochemical reaction causes the partial pressure of the water to exceed the saturated vapor pressure, causing liquid water to condense. The capillary force also causes liquid water to move toward the gas diffusion layer. Hence, this interface is the single-phase region when the saturation of the liquid water is 0. It becomes a two-phase region when the saturation of the liquid water exceeds 0. According to Fig. 2, to the right of the point where water condensation starts, a two-phase region is present along the flow channel. A single-phase region exists on the other side.

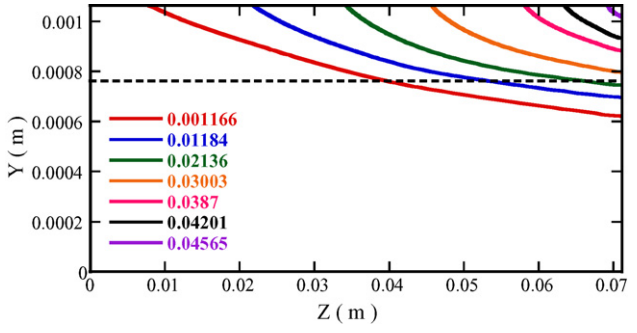

Fig. 7. Liquid water saturation field in the cathode gas channel and gas diffusion layer at a cell voltage of 0.7 V and a relative humidity of the cathode of 80%.

4. Conclusions

A multi-dimensional, multi-component, computational fluid dynamic model was developed to study the effect of the cathode humidification conditions on the location of the interface where the liquid water begins to condense along the flow channel in a PEM fuel cell. The model results support the following conclusions.

(1) The gas–liquid interface moves from the catalyst layer toward the diffusion layer as the relative humidity of the cathode increases. When the relative humidity of the cathode reaches 100%, the gas–liquid interface is close to the gas flow channel inlet.
(2) As the condensed water in the pores in the porous media blocks the transport of fuel gas, the cell performance and power density decrease as the relative humidity of the cathode increases.
(3) Reducing the cell operating voltage reduces the distance between the gas–liquid interface and the gas flow channel inlet, because the higher current is associated with a higher electrochemical reaction rate.
(4) The decreased oxygen fraction and the increased water fraction along the flow channel are related to the electrochemical reaction of the cathode catalyst layer, as oxygen is consumed and water produced.
(5) The transport of liquid water through the porous media is driven by the shear force of gas flow and the capillary force. Accordingly, liquid water moves from the catalyst layer toward the gas diffusion layer.

Acknowledgement

The authors would like to thank the National Science Council of the Republic of China, Taiwan, for financially supporting this research under Contract No. NSC 94-2212-E-009-001.

References

[1] C.Y. Wang, Chem. Rev. 104 (2004) 4727–4766.
[2] T. Okada, G. Xie, Y. Tanabe, J. Electroanal. Chem. 413 (1996) 49–65.
[3] D. Hyun, J. Kim, J. Power Sources 126 (2004) 98–103.
[4] T.E. Springer, T.A. Zawodzinski, S. Gottesfeld, J. Electrochem. Soc 138 (8) (1991) 2334–2342.
[5] T.E. Springer, M.S. Wilson, S. Gottesfeld, J. Electrochem. Soc. 140 (12) (1993) 3513–3526.
[6] T.F. Fuller, J. Newman, J. Electrochem. Soc. 140 (5) (1993) 1218–1225.
[7] T.V. Nguyen, R.E. White, J. Electrochem. Soc. 140 (8) (1993) 2178–2186.
[8] J.S. Yi, T.V. Nguyen, J. Electrochem. Soc. 145 (4) (1998) 1149–1159.
[9] S. Mazumder, J.V. Cole, J. Electrochem. Soc. 150 (11) (2003) A1503–A1509.

[10] S. Mazumder, J.V. Cole, J. Electrochem. Soc. 150 (11) (2003) A1510–A1517.
[11] Z.H. Wang, C.Y. Wang, K.S. Chen, J. Power Sources 94 (2001) 40–50.
[12] L. You, H. Liu, Int. J. Heat Mass Transfer 45 (2002) 2277–2287.
[13] H.C. Liu, W.M. Yan, C.Y. Soong, F. Chen, J. Power Sources 142 (2005) 125–133.
[14] C.Y. Soong, W.M. Yan, C.Y. Tzeng, H.C. Liu, F. Chen, H.S. Chu, J. Power Sources 143 (2005) 36–47.
[15] G. Lin, W. He, T.V. Nguyen, J. Electrochem. Soc. 151 (12) (2004) A1999–A2006.
[16] D. Natarajan, T.V. Nguyen, J. Power Sources 115 (2003) 66–80.
[17] W. He, J.S. Yi, T.V. Nguyen, AIChE J. 46 (10) (2000) 2053–2064.
[18] V. Gurau, H. Liu, S. Kakac, AIChE J. 44 (11) (1998) 2410–2422.
[19] S. Um, C.Y. Wang, Proceedings of the ASME Fuel Cell Division, November 5–10, 2000.